ACS OMEGA

Article

http://pubs.acs.org/journal/acsodf

Interfacial Activity of Gold Nanoparticles Coated with a Polymeric Patchy Shell and the Role of Spreading Agents

Miguel A. Fernández-Rodríguez,*[,†] Ana M. Percebom,[‡,§] Juan J. Giner-Casares,[‡] Miguel A. Rodríguez-Valverde,[†] Miguel A. Cabrerizo-Vílchez,[†] Luis M. Liz-Marzán,[‡,∥] and Roque Hidalgo-Álvarez[†]

[†]Biocolloid and Fluid Physics Group, Applied Physics Department, Faculty of Sciences, University of Granada, 18001 Granada, Spain

[‡]CIC biomaGUNE, Paseo de Miramón 182, 20009 Donostia-San Sebastián, Spain

[§]Department of Chemistry, Pontificia Universidade Catolica do Rio de Janeiro, Rua Marquês de São Vicente, 225, Rio de Janeiro, RJ 22451-900, Brazil

[∥]Ikerbasque, Basque Foundation for Science, 48013 Bilbao, Spain

Supporting Information

ABSTRACT: Gold patchy nanoparticles (PPs) were prepared under surfactant-free conditions by functionalization with a binary ligand mixture of polystyrene and poly(ethylene glycol) (PEG) as hydrophobic and hydrophilic ligands, respectively. The interfacial activity of PPs was compared to that of homogeneous hydrophilic nanoparticles (HPs), fully functionalized with PEG, by means of pendant drop tensiometry at water/air and water/decane interfaces. We compared interfacial activities in three different spreading agents: water, water/chloroform, and pure chloroform. We found that the interfacial activity of PPs was close to zero (~2 mN/m) when the spreading agent was water and increased to ~14 mN/m when the spreading agent was water/chloroform. When the nanoparticles were deposited with pure chloroform, the interfacial activity reached up to 60 mN/m by compression. In all cases, PPs exhibited higher interfacial activity than HPs, which were not interfacially active, regardless of the spreading agent. The interfacial activity at the water/decane interface was found to be significantly lower than that at the water/air interface because PPs aggregate in decane. Interfacial dilatational rheology showed that PPs form a stronger elastic shell at the pendant drop interface, compared to HPs. The significantly high interfacial activity obtained with PPs in this study highlights the importance of the polymeric patchy shell and the spreading agent.

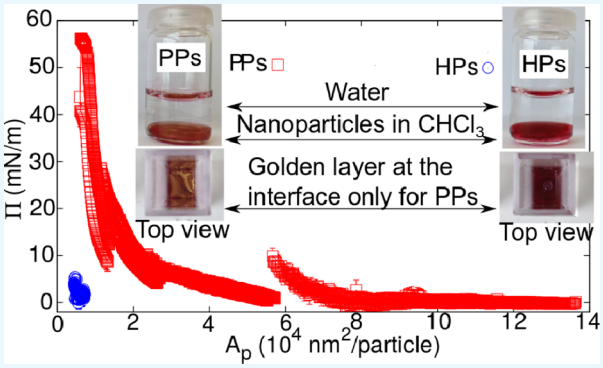

INTRODUCTION

Gold nanoparticles displaying interfacial activity are extensively studied as emulsion stabilizers due to the combination of the benefits of Pickering emulsions[1,2] and the plasmonic features of the Au cores.[3] One way to obtain this interfacial activity is to functionalize the nanoparticles with two different ligands with different wettabilities. If these ligands become segregated at the interface, the nanoparticle becomes a patchy nanoparticle (PP).[4−7] The presence of such patches of different wettabilities at the interface improves the ability of these nanoparticles to stabilize emulsions because of the spatial separation between the different wettability domains.[8] Moreover, it is possible to fine-control multiple anisotropy dimensions in such PPs,[9] which can lead to an anisotropic surface chemistry.[10] In the extreme case of only two domains of different wettabilities at the interface, a Janus nanoparticle (JP) is obtained and this spatial separation leads to enhanced interfacial activity as compared to homogeneous nanoparticles.[8,11] In fact, JPs have been predicted to show up to 3 times higher adsorption energy than their homogeneous counterparts, with randomly distributed capping ligands,[8] and even to produce thermodynamically stable Pickering emulsions.[12] These are not two exclusive synthesis paths; more complex synthesis can mix Janus and patchy morphologies in the same nanoparticle.[13] Thus, regardless of the Janus or patchy configuration, it is necessary to understand the role of the capping ligands that constitute the separate wettability domains of such JPs or PPs in their interfacial activity.[14]

Gold nanoparticles with thiol-terminated poly(ethylene glycol) (PEG) chains and short alkanethiols as capping ligands are efficient water/oil emulsion stabilizers.[1] Previous attempts to obtain gold nanoparticles functionalized by PEG and PS were made by Zubarev et al.,[15] where 2 nm diameter gold and silver cores were functionalized by V-shaped PS-*b*-PEG diblock

Received: July 18, 2016
Accepted: August 19, 2016
Published: August 31, 2016

DOI: 10.1021/acsomega.6b00131
ACS Omega 2016, 1, 311−317

Table 1. Results from Characterization of Each Nanoparticle System[a]

sample	polymer coating	core size (TEM)/nm	DLS size in H_2O/nm	solvent	occurrence of aggregation in bulk
13 nm PPs	PEG 1 kDa + PS 2 kDa	13 ± 1	220 ± 40	H_2O	yes
13 nm HPs	PEG 1 kDa	13 ± 1	50 ± 4	H_2O	no
23 nm PPs	PEG 1 kDa + PS 2 kDa	23 ± 2	230 ± 30	H_2O	yes
				$CHCl_3$	no
23 nm HPs	PEG 1 kDa	23 ± 2	47 ± 3	H_2O	no
				$CHCl_3$	no

[a]All results except mobility are from ref 4.

copolymers. Janus gold nanoparticles can also be obtained through the spontaneous segregation of two dissimilar polymers on the surface of the nanoparticle. The Janus character of these JPs was assessed by nuclear Overhauser effect spectroscopy-NMR (NOESY-NMR) and transmission electron microscopy (TEM) tomography images upon selective staining. As one hemisphere is coated with a hydrophilic polymer (polyethylene glycol (PEG)) and the other with a hydrophobic one (polystyrene (PS)), the nanoparticles can assemble into clusters with sizes that can be tuned by alterations in several parameters such as polymer length, polymer ratio, core size, and polarity of the medium.[4]

Interestingly, the spreading agent also plays a major role when the nanoparticles are deposited at fluid interfaces. This is because the evaporation of volatile spreading agents provides energy to the nanoparticles to reach and anchor at the interface. This process forms the so-called Langmuir monolayer, in contrast to a Gibbs monolayer in which the nanoparticles have to reach the interface from the bulk. The latter process is very slow as compared to the usual laboratory timescales and thus impractical in industrial processes.[14]

We present here an analysis of the importance of the polymeric capping ligands in gold nanoparticles, the size of the core, and the spreading agent used during the deposition at water/air and water/decane interfaces. We used pendant drop tensiometry to compare the interfacial activity of gold PPs of 13 and 23 nm nanoparticles functionalized with PS (2 kDa) and PEG (1 kDa) with that of homogeneous nanoparticles functionalized with PEG only. The role of the spreading agent was studied by comparing the behavior in pure water, water/$CHCl_3$, and pure $CHCl_3$. Finally, particle-laden interfaces were studied by interfacial dilatational rheology to study the microstructure of the nanoparticles at the pendant drop interface.

METHODS

Preparation of PPs. The nanoparticles investigated in this study were prepared by using the methodology reported in ref 4. In brief, gold nanoparticles were synthesized by reduction of $HAuCl_4$ by sodium citrate and were then added to a solution of thiol-terminated polymers for coating. Whereas for the synthesis of hydrophilic nanoparticles (HPs) an aqueous solution of PEG-SH or PS-SH was used, PPs were obtained with an equimolar mixture of PEG-SH and PS-SH in tetrahydrofuran (THF). The main difference between the preparation of the nanoparticles in this study and that in ref 4 was the purification process. To guarantee that no traces of citrate, free polymer, or THF remained in the sample, centrifugation and supernatant exchange were repeated 5-fold in this study. No impurities with significant surface activity were observed.

Characterization of Nanoparticles. As described in ref 4, the NOESY-NMR spectra (NOESY, Bruker 500 MHz spectrophotometer) of the nanoparticles synthesized with the equimolar mixture of PEG-SH of 1 kDa and PS-SH of 2 kDa revealed a significant segregation of the polymers at the nanoparticle surface, that is, a patchy morphology. These nanoparticles were characterized by TEM (JEOL 2010F FEG-TEM) and dynamic light scattering (DLS) (Malvern Zetasizer Nano) to obtain information regarding the sizes of individual nanoparticles and their assemblies in bulk solution. Table 1 summarizes the obtained results where the occurrence of aggregation in bulk refers to the formation of clusters in each corresponding solvent. The homogeneous nanoparticles functionalized by PS-SH were too hydrophobic to be dispersed in water. Thus, we considered only the Janus and hydrophilic homogeneous nanoparticles. Both hydrophilic homogeneous and PPs were negatively charged when dispersed in water, whereas the hydrophobic homogeneous nanoparticles could not be measured in water.

The core size of the hydrophobic PS-capped nanoparticles was 17 ± 3 nm (by TEM) and the core plus polymeric shell size was 30 ± 4 nm (by DLS) in organic solvents ($CHCl_3$ and THF).

Electron microscopy analyses with either staining or chemical modification of the PEG-patch revealed that the polymeric shell assumes a Janus configuration for various pairs of polymers (PEG 5 kDa + PS 2 kDa and PEG 1 kDa + PNIPAM 1.2 kDa in different proportions).[4] However, due to the assembly of nanoparticles coated by PEG 1 kDa + PS 2 kDa in water, it was not possible to apply the same analysis for the system of this study. Therefore, we can only confirm that PEG 1 kDa and PS 2 kDa are segregated on the nanoparticle surface in a patchy conformation.

Pendant Drop Tensiometry. We used a homemade setup described in a previous report.[16] We started by depositing a given amount of nanoparticle dispersion with a microsyringe on a 20 μL Milli-Q water pendant drop in air. Next, the pendant drop volume was increased up to 45 μL and the surface tension was monitored while keeping the drop volume constant over time. The fall of the pendant drop due to low-tension values was prevented using a bigger poly(tetrafluoroethylene) capillary with a cap (with external diameters of 2.8 and 4.2 mm for the capillary and the cap, respectively, see Figure 1). We monitored the surface tension (γ) over time for these experiments.

After 20 min, the surface tension was stable over time in most cases. Next, we performed growing and shrinking cycles in air by varying the total volume of the drop between 45 and 15 μL at the lowest rate possible with our setup, 0.08 μL/s. When pure $CHCl_3$ was used as the spreading solvent, the evaporation process was violent and completed in a few seconds (see Figure 1). When water/$CHCl_3$ was used as the spreading agent, half of the microsyringe was loaded with the aqueous nanoparticle

DOI: 10.1021/acsomega.6b00131
ACS Omega 2016, 1, 311−317

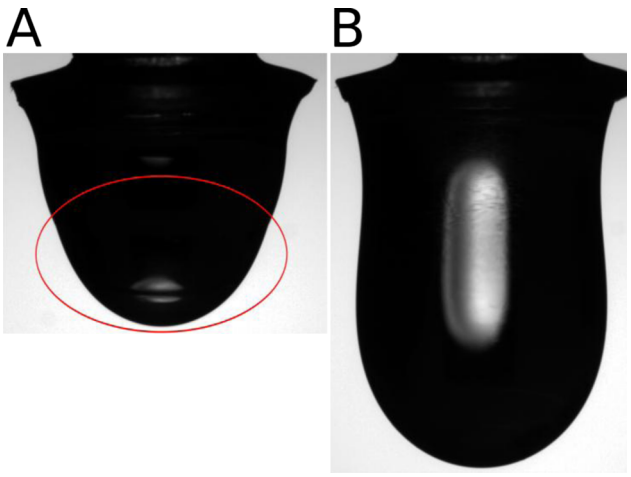

Figure 1. (A) Water pendant drop (20 μL) in air with 5.9×10^9 PPs of 23 nm diameter deposited using $CHCl_3$ as the spreading agent. Note the $CHCl_3$ on the bottom of the pendant drop indicated by the red circle. (B) Water pendant drop (45 μL); the same pendant drop as in (A); after evaporation of $CHCl_3$, this pendant drop fell off because of the low surface tension.

dispersion and half with $CHCl_3$. We also performed growing and shrinking experiments at the water/decane interface by shrinking the pendant drop to 10 μL, immersing in decane, and then growing again up to 45 μL. Finally, the same growing and shrinking cycles were performed in contact with the decane phase. For these experiments, the surface pressure was plotted, defined as $\Pi = \gamma_0 - \gamma$, where γ_0 is 72.5 and 52.3 mN/m for water/air and water/decane interfaces, respectively, and γ is the surface tension measured with nanoparticles. The surface pressure was plotted against either the pendant drop area or the area per particle A_p (the area of the pendant drop divided by the number of deposited nanoparticles).

Dilatational interfacial rheology was carried out as described in a previous work,[17] by growing and shrinking the pendant drop at different periods with a fixed 1 μL amplitude. From the differences in amplitude and phase of the input volume oscillation and the output surface tension, it is possible to obtain the interfacial elastic modulus E_d and viscosity η_d, in analogy to the storage and loss moduli in three-dimensional rheology.

RESULTS AND DISCUSSION

Effect of the Spreading Agent. The role of the spreading agent was studied by depositing a given amount of 13 nm PPs at the water/air interface. Experiments were carried out using either only water as the solvent or loading the microsyringe half with the aqueous nanoparticle dispersion and half with chloroform ($CHCl_3$). The interfacial activity was determined to be close to zero (~2 mN/m for the highest compression state) when the aqueous colloid was deposited (see Figure 2), whereas it increased up to ~14 mN/m when water/$CHCl_3$ was used as the spreading solvent. The absence of surface-active impurities in the $CHCl_3$ used as the spreading agent was confirmed, as shown in the black curve in Figure 2a, which corresponds to the deposition of 5 μL of pure $CHCl_3$. Chloroform was selected as the spreading agent due to an effect observed when the PPs were dispersed in $CHCl_3$ and water was added to the dispersion. As chloroform and water are immiscible and the former is denser, the addition of water

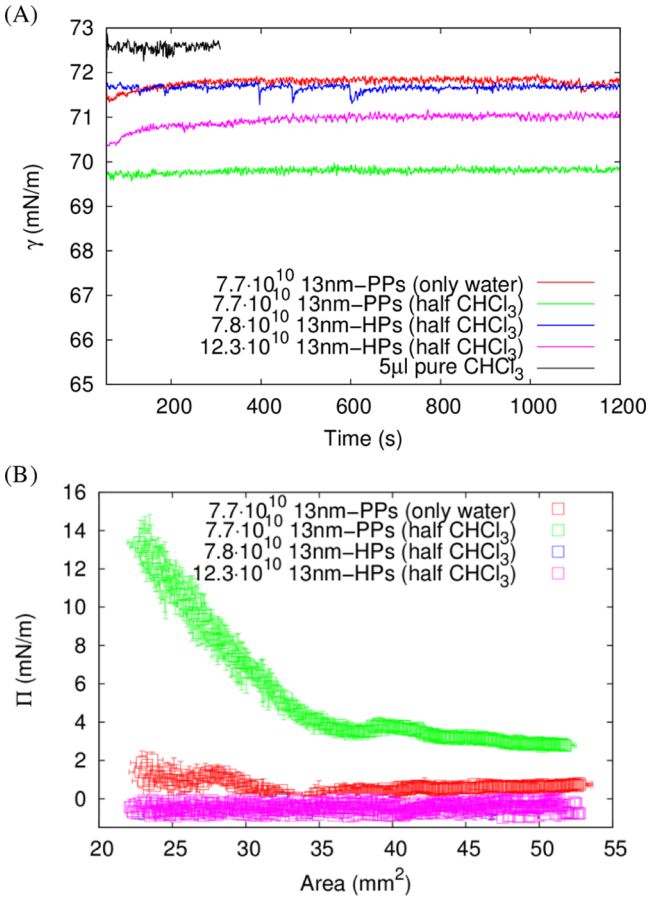

Figure 2. (A) Evolution of surface tension γ over time, after deposition of 13 nm PPs and HPs at the water/air interfaces with different spreading agents (pure water or water/$CHCl_3$). (B) Surface pressure Π vs area of the growing and shrinking cycles for (A) curves. The black curve in (A) corresponds to the evaporation of pure $CHCl_3$ deposited at the interface to test the purity of the spreading solvent.

generates an upper phase. Interestingly, a metallic gold-like layer was observed at the interface when PPs were present in the bottom phase (see Figure 3), indicating that they tend to self-assemble at the $CHCl_3$/water interface. The golden layer, which only occurs with PPs at the $CHCl_3$/water interface, may be pointing out that their interfacial activity produces a high population at the interface, with a high interfacial pressure. A study of this interface at the pendant drop would help explain

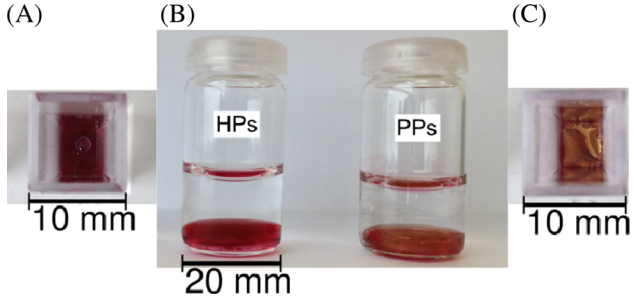

Figure 3. Digital photographs of samples of nanoparticles dispersed in chloroform in the presence of an extra upper water phase (B). The interface between both phases does not change color for homogeneous nanoparticles (A), but it becomes golden-like for PPs (C). The insets show top views of the same samples in square cuvettes.

DOI: 10.1021/acsomega.6b00131
ACS Omega 2016, 1, 311−317

this effect better. However, the formation of a chloroform pendant drop in water produced a profile not analyzable by axisymmetric drop shape analysis (see Figure S1). On the other hand, HPs did not display this assembly behavior. From this observation, we expected that chloroform would be an efficient spreading agent for this system. The observed interfacial activity difference can be explained in terms of the formation of a Langmuir monolayer versus a Gibbs monolayer.[14] When PPs are deposited from water, they join the water subphase and a Gibbs monolayer is formed by which PPs reach the pendant drop interface very slowly.[14] This is especially unfavorable for nanoparticles with sizes of a few nanometers in which the adsorption energy is in the range of k_BT.[18] In contrast, when water/$CHCl_3$ is used as the spreading agent, the abrupt evaporation of $CHCl_3$ promotes the formation of a Langmuir monolayer in which the nanoparticles can reach the interface at a much faster rate, which is evidenced by the stable surface tension, as shown in Figure 2a. Concerning the comparison of interfacial activity between homogeneous and PPs, 13 nm HPs showed no interfacial activity compared to 13 nm PPs (see Figure 2a,b), even for higher concentrations of 13 nm HPs and while using water/$CHCl_3$ as the spreading agent. As PS ligands are hydrophobic but PEG is hydrophilic, 13 nm HPs functionalized only with PEG are expected to be more hydrophilic and tend to stay in the water subphase, provided the hydrodynamic radius in water obtained by DLS for HPs in Table 1. On the other hand, the interfacial activity of the 13 nm PPs is expected to arise from the patchy character of these nanoparticles with hydrophobic PS domains. Although the HPs show a very low interfacial activity that might be caused by either pollution or particle size, it is clear that the surface tension and surface pressure upon compression are significantly lower than those corresponding to PPs. Both PPs and HPs are not enough to provide a close-packed monolayer; however, in the case of PPs deposited with half chloroform, the higher interfacial activity may be explained in terms of a percolating network of aggregates at the interface that increase the surface pressure upon compression of the interface.

Nanoparticles Dispersed in an Organic Solvent. We additionally explored the possibility of increasing the interfacial activity by redispersing the PPs in pure $CHCl_3$ and increasing their size. The nanoparticle size is an important factor in the interfacial adhesion energy E_{ads} at interfaces, which follows eq 1,[8] where R is the radius of the particle, γ_{12} is the surface tension of the bare fluid−fluid interface, and θ_{12} is the three-phase contact angle.

$$E_{ads} = \pi R^2 \gamma_{12}(1 \pm \cos\theta_{12})^2 \quad (1)$$

$E_{ads} \propto R^2$ is more than 3 times higher for 23 nm nanoparticles than for 13 nm nanoparticles. Therefore, bigger nanoparticles are expected to be more firmly anchored at the interface. If we use eq 1 with γ_{12} = 72.5 mN/m for the water/air interface and we consider θ_{12} = 90° (to provide the highest E_{ads}), E_{ads} = 2341 kT for the 13 nm nanoparticles and 7329 kT for the 23 nm nanoparticles, at T = 25 °C. Thus, if we consider the high energy of adsorption of the nanoparticles and the fact that we are providing extra energy from the violent process of evaporation of the spreading solvent, it might be plausible to consider that all nanoparticles became placed at the interface, while we do not know exactly the microstructure. We first characterized the water/air interface, as shown in Figure 4. The black curve in Figure 4a corresponds to the supernatant

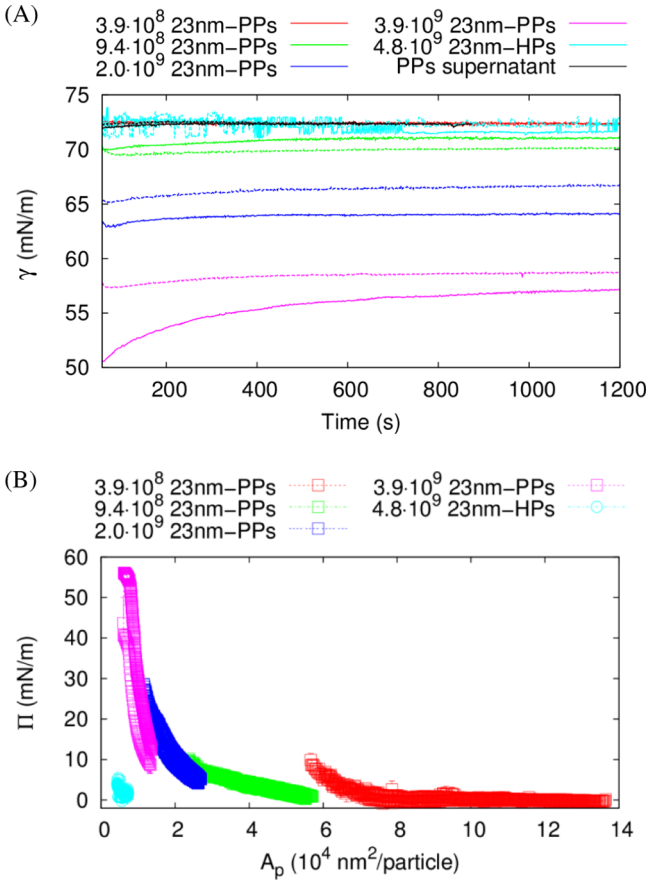

Figure 4. (A) Evolution of the interfacial tension (γ) over time upon deposition of 23 nm PPs (squares) and HPs (circles) dispersed in $CHCl_3$ (which is used as the spreading agent) at water/air interfaces. (B) Surface pressure Π vs A_p of the growing and shrinking cycles corresponding to the curves in (A). The black curve in (A) corresponds to the evaporation of 1 μL of the supernatant from 23 nm PPs dispersed in $CHCl_3$ after centrifugation, to test that the $CHCl_3$ is not desorbing the polymers from the 23 nm PPs.

obtained after centrifugation of the 23 nm PPs at 5500g for 30 min in a glass tube (to avoid $CHCl_3$ from dissolving the plastic centrifugation tube). It can be seen that the supernatant was clean, therefore recovering the interfacial activity of a bare water/air interface (~72.5 mN/m). This indicates that the redispersion in $CHCl_3$ did not lead to desorption of the polymers or contaminate the nanoparticle dispersion. Figure 4a shows that the final stable surface tension after $CHCl_3$ evaporation increased with the concentration of 23 nm PPs and was reproducible for two separate runs (solid and dashed lines for each color in Figure 4a), whereas 23 nm HPs dispersed in water exhibited no interfacial activity for even higher concentrations, as expected. Thus, 23 nm HPs serve as a control case for nanoparticles with no interfacial activity. In Figure 4b, the growing and shrinking cycles performed for the different initial concentrations enabled building of a piecewise-like compression isotherm (see Figure S2 to see pictures of the pendant drops). At high values of surface area between 8×10^4 nm^2/particle and 14×10^4 nm^2/particle, the surface pressure Π starts at zero and increases upon decreasing A_p (i.e., increasing the compression state) up to ~60 mN/m, which is the highest reported surface pressure with nanometer-sized gold PPs, to the best of our knowledge. This value is significantly higher than the maximum value $\Pi \sim 20$ mN/m reported with 4 nm gold

DOI: 10.1021/acsomega.6b00131
ACS Omega 2016, 1, 311−317

true JPs half-functionalized with hexanethiol and half with 2-(2-mercapto-ethoxy)ethanol and dispersed in THF,[17] which is a special case of 2-patch nanoparticles. Therefore, the realization of a Langmuir monolayer by PPs is demonstrated. Additionally, a change in the slope is visible in Figure 4b, around $A_p = 10^4$ nm^2/particle, which has also been reported for silver JPs by Fernández-Rodríguez et al.[16] In the present case, we do not have enough particles to obtain a close-packed monolayer, but it is likely that the change in slope is due to nanoparticles coming in contact by percolating domains in a fractal-like manner, as observed by several authors for JPs.[19,20]

Finally, the interfacial activity of 23 nm PPs is compared to that of 23 nm HPs for higher concentrations. As can be seen in Figure 4b, the 23 nm HPs show no interfacial activity, as compared to the value of $\Pi \sim 60$ mN/m for 23 nm PPs. This is a clear evidence that the combination of size and polymers used to synthesize the 23 nm PPs leads to a significantly higher interfacial activity than that of homogeneous nanoparticles. Moreover, when we synthesized particles with a bigger PEG of 5 kDa (results not shown), we never obtained interfacial activity, either for HPs or for particles with two polymers (PEG of 5 kDa and PS of 2 kDa), probably because the long PEG chains render the nanoparticles significantly hydrophilic and very stable in the aqueous bulk. The foamability of similar nanoparticles was previously reported by Hunter and Jameson, who studied the adsorption of 120 and 300 nm PS nanoparticles functionalized by PEG monomethacrylate (PEGMA) at the water/air interface,[21] so that PEGMA functionalization provided steric stabilization to the nanoparticles. The highest surface pressure obtained for the 300 nm particles greatly depended on the pH of the water subphase: 27 mN/m for pH 2 and 7 mN/m for pH 6, because these nanoparticles are strongly positively charged at pH 2, and uncharged at pH 6 (producing aggregation of the nanoparticles). A similar behavior was found for the 120 nm nanoparticles (22−25 mN/m at pH 2). These nanoparticles showed a good ability to produce foams, with good agreement between the Langmuir trough experiments at the water/air interface and the foaming behavior: lower pH leads to stronger adsorption and formation of a more robust steric barrier. Nevertheless, our 23 nm PPs present a clearly enhanced interfacial activity, which points out the importance of choosing the right polymers and the right solvents.

Interfacial Dilatational Rheology. One way to study the microstructure of the nanoparticles deposited at the pendant drop interface is to perform interfacial dilatational rheology experiments, from which we can see the response of the nanoparticles at the pendant drop interface toward periodic increments and reductions of the available A_p. Figure 5 shows that E_d is of 1 order of magnitude larger than η_d for each A_p studied, pointing out a solid elastic-shell behavior. E_d decreases and η_d increases with the period because for higher periods, the perturbation is lower and the surface shows less elastic behavior. There is a clear trend of increasing E_d and η_d for decreasing A_p for the 23 nm PPs, showing the elastic-shell behavior that becomes more important as there are more particles per unit of area. On the other hand, the 23 nm HPs at higher concentrations show once more no interfacial activity through lack of elasticity and viscosity, similar to a bare water/air interface. This elastic-shell behavior in which the elastic modulus increases from 25 up to 450 mN/m points out the interfacial activity of PPs and their capability as foam stabilizers

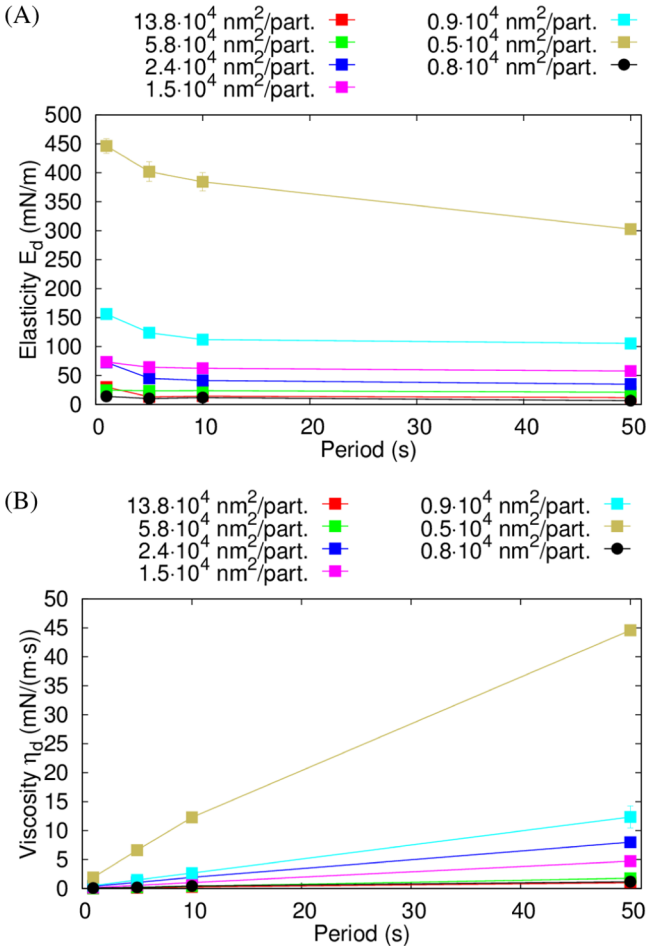

Figure 5. (A) Interfacial dilatational elastic modulus (E_d) and (B) viscosity (η_d) of 23 nm PPs (squares) and HPs (circles) dispersed in $CHCl_3$ against different periods for different A_p compression states at the water/air interface.

(see Figure S3 to see drop pictures during the interfacial dilatational rheology).

Surface Tension at the Liquid/Liquid Interface. The interfacial activity at liquid/liquid interfaces was studied by immersing the pendant drop in decane for the highest concentrations measured with 23 nm PPs (see Figure 6). The interfacial activity of the pendant drop immersed in decane is close to zero. No interfacial activity was observed for the 23 nm HPs both at water/air and at water/decane interfaces. The immersion of the pendant drop in decane is likely to produce aggregation of the nanoparticles, leading to a low interfacial activity in water/decane compared to water/air interfaces. However, from previous works with a similar methodology and true Janus gold nanoparticles (4 nm diameter; functionalized with hexanethiol and mercaptoethoxyethanol),[17] similar values of surface tension were measured at water/air and water/decane interfaces for similar A_p. Thus, the difference of interfacial activity of 23 nm PPs at water/air and water/decane interfaces is expected to arise from either the particle size or the polymers. From eq 1, E_{ads} is calculated to be 33 times higher for 23 nm gold nanoparticles than for 4 nm nanoparticles in ref 17, and therefore the bigger particles are expected to better withstand the immersion in decane. This suggests that the polymers are responsible for the interfacial activity differences at water/air and water/decane interfaces. Transfer of the PPs

DOI: 10.1021/acsomega.6b00131
ACS Omega 2016, 1, 311−317

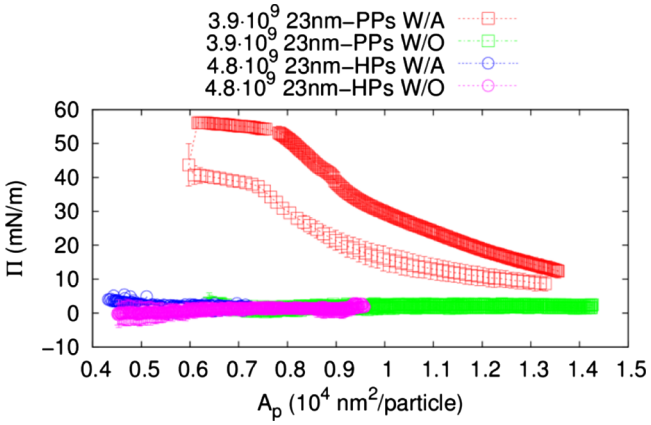

Figure 6. Π vs A_p for the growing and shrinking cycles of 23 nm PPs (squares) and HPs (circles) dispersed in $CHCl_3$ at water/air (solid lines) and water/decane (dashed lines) interfaces. Note that for the red squares, the upper curve corresponds to shrinking, whereas the lower curve corresponds to the growth of the pendant drop.

into decane was not successful, as they irreversibly aggregated and precipitated. Thus, the aggregation hypothesis is the most likely one. In any case, this is evidence that not all nanoparticles that show a high interfacial activity at water/air interfaces also show a high interfacial activity at water/oil interfaces (see Figure S4 to see a comparison between the water drops in air and after immersion in decane).

This behavior was reproduced by using interfacial dilatational rheology (Figure 7), showing that elasticity and viscosity are always greater for water/air (solid lines) than for water/decane interfaces (dashed lines). Moreover, for water/air interfaces, when the pendant drop is shrunk, the elasticity and viscosity increase significantly as explained above.

To better understand the microstructure of fluid interfaces covered with functionalized gold nanoparticles it would be necessary to employ techniques such as X-rays or electron diffraction.[22−25] In particular, these ultrafast techniques would provide new insights into the microstructure at the interface in out-of-equilibrium conditions.

CONCLUSIONS

The interfacial activity of gold PPs in the range 13−23 nm, synthesized under surfactant-free conditions, was studied by pendant drop tensiometry. The particles are functionalized with PS (2 kDa) and PEG (1 kDa) as hydrophobic and hydrophilic polymers presenting a patchy morphology at the surface, respectively. Homogeneous HPs fully functionalized with PEG were synthesized to compare the interfacial activity with the corresponding PPs. The HPs exhibited no interfacial activity compared to the PPs, pointing out the ability of the latter as better foam stabilizers. Moreover, we tested the efficiency of water, a water/$CHCl_3$ mixture and pure $CHCl_3$ as spreading agents, and the better spreading agent was pure $CHCl_3$ reaching surface pressure values of 60 mN/m at the water/air interface. Under these conditions, the water/air interface behaved as an elastic shell, which additionally pointed out the ability of these PPs as foam stabilizers. Finally, the interfacial activity was found to be close to zero when the pendant drops were immersed in decane, which might be due to irreversible aggregation of the nanoparticles during immersion in decane. Thus, the roles of the polymers and spreading agent were

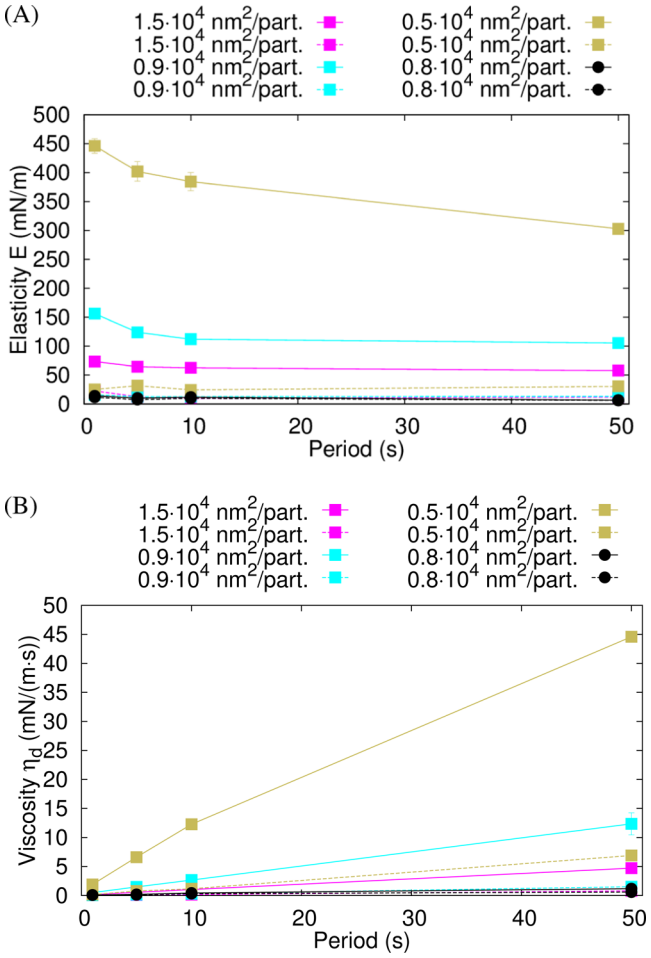

Figure 7. (A) Interfacial dilatational elastic modulus (E_d) and (B) viscosity (η_d) of 23 nm PPs and HPs dispersed in $CHCl_3$ against different periods for different A_p compression states at the water/air (solid lines) and water/decane (dashed lines) interfaces.

revealed to be crucial when PPs with high interfacial activity are to be spread on a specific interface.

ASSOCIATED CONTENT

Supporting Information

The Supporting Information is available free of charge on the ACS Publications website at DOI: 10.1021/acsomega.6b00131.

Further images of pendant drop tensiometry with PPs deposited at the interface (PDF)

AUTHOR INFORMATION

Corresponding Author

*E-mail: mafernandez@ugr.es.

Notes

The authors declare no competing financial interest.

ACKNOWLEDGMENTS

This work was supported by the Spanish MINECO (projects MAT2013-44429-R and MAT2014-60615R), by "Junta de Andalucía" and FEDER (projects P10-FQM-5977 and P12-FQM-1443), by the European Research Council (ERC Advanced Grant #267867 Plasmaquo), and by the Brazilian Funding Agency FAPESP (2012/21930-3 and 2014/01807-8). J.J.G.-C. acknowledges the Ministry of Economy and

DOI: 10.1021/acsomega.6b00131
ACS Omega 2016, 1, 311−317

Competitiveness for a Juan de la Cierva fellowship (#JCI-2012-12517). The authors thank Drs. J. A. Holgado-Terriza and J. L. Muros-Cobos for the software Contacto© used for surface tension measurements.

REFERENCES

(1) Larson-Smith, K.; Pozzo, D. C. Pickering Emulsions Stabilized by Nanoparticle Surfactants. *Langmuir* **2012**, *28*, 11725−11732.
(2) Binks, B. P. Particles as surfactants-similarities and differences. *Curr. Opin. Colloid Interface Sci.* **2002**, *7*, 21−41.
(3) Gorgoll, R. M.; Tsubota, T.; Harano, K.; Nakamura, E. Cooperative Self-Assembly of Gold Nanoparticles on the Hydrophobic Surface of Vesicles in Water. *J. Am. Chem. Soc.* **2015**, *137*, 7568−7571.
(4) Percebom, A. M.; Giner-Casares, J. J.; Bals, S.; Loh, W.; Liz-Marzán, L. M. Janus gold nanoparticles obtained via spontaneous binary polymer shell segregation. *Chem. Commun.* **2016**, *52*, 4278−4281.
(5) Sosa, C.; Liu, R.; Tang, C.; Qu, F.; Niu, S.; Bazant, M. Z.; Prud'homme, R. K.; Priestley, R. D. Soft Multifaced and Patchy Colloids by Constrained Volume Self-Assembly. *Macromolecules* **2016**, *49*, 3580−3585.
(6) Bradley, L.; Zhao, Y. Uniform Plasmonic Response of Colloidal Ag Patchy Particles Prepared by Swinging Oblique Angle Deposition. *Langmuir* **2016**, *32*, 4969−4974.
(7) Ku, K. H.; Kim, Y. J.; Yi, G.-R.; Jung, Y. S.; Kim, B. J. Soft Patchy Particles of Block Copolymers from Interface-Engineered Emulsions. *ACS Nano* **2015**, *9*, 11333−11341.
(8) Binks, B. P.; Fletcher, P. D. I. Particles Adsorbed at the Oil-Water Interface: A Theoretical Comparison between Spheres of Uniform Wettability and Janus Particles. *Langmuir* **2001**, *17*, 4708−4710.
(9) Pawar, A. B.; Kretzschmar, I. Multifunctional Patchy Particles by Glancing Angle Deposition. *Langmuir* **2009**, *25*, 9057−9063.
(10) Burrows, N. D.; Vartanian, A. M.; Abadeer, N. S.; Grzincic, E. M.; Jacob, L. M.; Lin, W.; Li, J.; Dennison, J. M.; Hinman, J. G.; Murphy, C. J. Anisotropic Nanoparticles and Anisotropic Surface Chemistry. *J. Phys. Chem. Lett.* **2016**, *7*, 632−641.
(11) Lenis, J.; Razavi, S.; Cao, K. D.; Lin, B.; Lee, K. Y. C.; Tu, R. S.; Kretzschmar, I. J. Mechanical Stability of Polystyrene and Janus Particle Monolayers at the Air/Water Interface. *J. Am. Chem. Soc.* **2015**, *137*, 15370−15373.
(12) Aveyard, R. Can Janus particles give thermodynamically stable Pickering emulsions? *Soft Matter* **2012**, *8*, 5233−5240.
(13) McConnell, M. D.; Kraeutler, M. J.; Yang, S.; Composto, R. J. Patchy and Multiregion Janus Particles with Tunable Optical Properties. *Nano Lett.* **2010**, *10*, 603−609.
(14) Garbin, V.; Crocker, J. C.; Stebe, K. J. Nanoparticles at fluid interfaces: Exploiting capping ligands to control adsorption, stability and dynamics. *J. Colloid Interface Sci.* **2012**, *387*, 1−11.
(15) Zubarev, E. R.; Xu, J.; Sayyad, A.; Gibson, J. D. Amphiphilicity-Driven Organization of Nanoparticles into Discrete Assemblies. *J. Am. Chem. Soc.* **2006**, *128*, 15098−15099.
(16) Fernández-Rodríguez, M. A.; Rodriguez-Valverde, M. A.; Cabrerizo-Vilchez, M.; Hidalgo-Alvarez, R. Surface activity and collective behaviour of colloidally stable Janus-like particles at the air−water interface. *Soft Matter* **2014**, *10*, 3471−3476.
(17) Fernandez-Rodriguez, M. A.; Chen, L.; Deming, C. P.; Rodriguez-Valverde, M. A.; Chen, S.; Cabrerizo-Vilchez, M.; Hidalgo-Alvarez, R. A simple strategy to improve the interfacial activity of true Janus gold nanoparticles: a shorter hydrophilic capping ligand. *Soft Matter* **2016**, *12*, 31−34.
(18) Ferdous, S.; Ioannidis, M.; Henneke, D. Adsorption kinetics of alkanethiol-capped gold nanoparticles at the hexane-water interface. *J. Nanopart. Res.* **2011**, *13*, 6579−6589.
(19) Walther, A.; Müller, A. H. E. Janus Particles: Synthesis, Self-Assembly, Physical Properties, and Applications. *Chem. Rev.* **2013**, *113*, 5194−5261.
(20) Fernandez-Rodriguez, M. A.; Ramos, J.; Isa, L.; Rodriguez-Valverde, M. A.; Cabrerizo-Vilchez, M. A.; Hidalgo-Alvarez, R. Interfacial Activity and Contact Angle of Homogeneous, Functionalized, and Janus Nanoparticles at the Water/Decane Interface. *Langmuir* **2015**, *31*, 8818−8823.
(21) Hunter, T. N.; Jameson, G. J.; Wanless, E. J.; Dupin, D.; Armes, S. P. Adsorption of Submicrometer-Sized Cationic Sterically Stabilized Polystyrene Latex at the Air-Water Interface: Contact Angle Determination by Ellipsometry. *Langmuir* **2009**, *25*, 3440−3449.
(22) Ruan, C. Y.; Murooka, Y.; Raman, R. K.; Murdick, R. A. Dynamics of Size-Selected Gold Nanoparticles Studied by Ultrafast Electron Nanocrystallography. *Nano Lett.* **2007**, *7*, 1290−1296.
(23) Clark, J. N.; Beitra, L.; Xiong, G.; Higginbotham, A.; Fritz, D. M.; Lemke, H. T.; Zhu, D.; Chollet, M.; Williams, G. J.; Messerschmidt, M.; Abbey, B.; Harder, R. J.; Korsunsky, A. M.; Wark, J. S.; Robinson, I. K. Ultrafast Three-Dimensional Imaging of Lattice Dynamics in Individual Gold Nanocrystals. *Science* **2013**, *341*, 56−59.
(24) Latychevskaia, T.; Mancini, G. F.; Carbone, F. The role of the coherence in the cross-correlation analysis of diffraction patterns from two-dimensional dense mono-disperse systems. *Sci. Rep.* **2015**, *5*, 16573.
(25) Mancini, G. F.; Latychevskaia, T.; Pennacchio, F.; Reguera, J.; Stellacci, F.; Carbone, F. Order/Disorder Dynamics in a Dodecanethiol-Capped Gold Nanoparticles Supracrystal by Small-Angle Ultrafast Electron Diffraction. *Nano Lett.* **2016**, *16*, 2705−2713.

DOI: 10.1021/acsomega.6b00131
ACS Omega 2016, 1, 311−317